

Electrochemical Performance of Mn₃O₄/G/CB Composite Materials for Supercapacitors

Liquan Lu^{1,*}, Shengming Xu², Junwei An²

¹ School of Mechatronics Engineering, North University of China, Taiyuan 030051, China

² Institute of Nuclear and New Energy Technology, Tsinghua University, Beijing 100084, China

*E-mail: lq_lu@buaa.edu.cn

Received: 4 April 2016 / Accepted: 18 May 2016 / Published: 4 June 2016

In this paper, a new type of supercapacitor electrode material is synthesized using graphene, carbon black and Mn₃O₄ (Mn₃O₄/G/CB). This composite material can make full use of the high conductivity of the graphene and the high specific surface area of the carbon black to improve the conductivity, specific capacitance and cycle stability of the Mn₃O₄. At 0.1A/g current density, the specific capacitance of the Mn₃O₄/G/CB composite is 661F/g, which is 4 times higher than that of Mn₃O₄ (165F/g) under the same current density. The CV curves of the Mn₃O₄/G/CB composite are maintained in the shape of an approximately rectangular shape, and have a fast current response rate. Under the high current density of 30A/g, after 5000 cycles of charge-discharge test, 69.2% of the initial specific capacitance is still retained for the Mn₃O₄/G/CB composite, while the specific capacitance of the Mn₃O₄ only remains 63.6%, after the same process. According to the EIS test, the charge transfer resistance and Warburg resistance of the Mn₃O₄/G/CB composites are all less than Mn₃O₄, which is attributed to the addition of the graphene and carbon black.

Keywords: Supercapacitor; Mn₃O₄; Carbon black; Graphene; Electrode Materials

1. INTRODUCTION

It is believed that the manganese oxides are the most promising pseudo capacitance materials in the supercapacitor electrode materials, because of their characterization of the low cost, rich in nature, and friendly environment [1-3]. Compared with other manganese oxides, Mn₃O₄ has a single hausmannite structure at room temperature, and it is the most stable manganese oxide [4,5]. Therefore, the pure Mn₃O₄ phase with the neat microstructure is easily obtained. However, the electrical conductivity and cycle stability of Mn₃O₄ are very poor, and the specific power of Mn₃O₄ is very small. Thus, numerous research workers try to compound the Mn₃O₄ with some carbon materials with

high electrical conductivity and cycle stability to synthesize the composite materials with good electrochemical performance [5]. Graphene with high conductivity, large surface area and good chemical stability has been widely studied in the preparation of the electrode composite materials for supercapacitors [6-12]. Using a modified Hummers method, Qu et al. prepared a composite material using the reduced graphene oxide and Mn_3O_4 (G/ Mn_3O_4), whose specific capacitance reaches 284 F/g at the current density of 50 mA/g [13]. However, the specific capacitance and cycle ability of the Mn_3O_4 composites need to be raised for a further level. Moreover, carbon black (CB) produced by industrialized is a popular carbon material with high conductivity and excellent chemical stability [14]. It also has been widely employed as the conductive additives for lithium batteries and the electrode materials in the supercapacitor [15,16].

In this study, a spherical CB with high specific surface area is employed to further enhance the specific capacitance and cycle stability of G/ Mn_3O_4 composite. The Mn_3O_4 /G/CB composites are characterized by TEM and XRD. The electrochemical performance of the Mn_3O_4 /G/CB composites is investigated using cyclic voltammetry, galvanostatic charge–discharge (GCD) and electrochemical impedance spectroscopy (EIS). The testing results indicate that the conductivity and cycle stability of the Mn_3O_4 are improved greatly, due to the close integration of the CB, graphene and Mn_3O_4 , which causes the high conductivity of the graphene is fully brought into play, resulting in the pseudo capacitance of the Mn_3O_4 are fully excavated.

2. EXPERIMENTAL

2.1 Preparation of the graphene

The graphene oxide is prepared by a modified Hummers method [17]. The preparation processes are as follows: firstly, 25 g sodium nitrate, 50 g expandable graphite and 500 ml concentrated sulfuric acid are added in a 2 l beaker, which is put in a water bath whose temperature is fixed at 0 °C, to prevent its temperature from rising to 10 °C. Then, 300 g potassium permanganate is added into the mixture in 6 times under gently stirring within 1 h. After that, the temperature of the mixture is risen to 35 °C. 30 min later, 920 ml distilled water is slowly dropped into the mixture. After further stirring for 1 h, the solution is set quietly for 12 h. Then, it is heated to 98 °C. 1 h later, the resulting brown solution is washed and filtrated. After the residue is dried, a graphene oxide can be obtained.

In a flask, 0.65 g graphene oxide prepared above is dispersed in 0.5 l acetic acid by ultrasonic agitation for 30 min. Then the flask is placed in a water bath, in which the temperature is fixed at 30 °C. After that, 15 ml hydriodic acid is added to the flask. After 40 h of reaction, saturated sodium bicarbonate solution is added to the mixture for neutralization. Afterwards, the mixture is washed and filtrated. The reduced graphene prepared using hydriodic acid as the reducing reagent is obtained, after the filter residue is dried in a vacuum oven for 12 h at 80 °C.

2.2 Preparation of the $Mn_3O_4/G/CB$ composites

The synthesizing procedures of the $Mn_3O_4/G/CB$ composites are as follows: firstly, 0.875 g manganous acetate, 3.35 g oleyl amine, 0.71 g oleic acid, 0.05 g graphene and 0.03 g carbon black are added into a flask, successively. Then, the mixture is stirred using ultrasonic for 15 min. After that, the flask is placed in a water bath, whose temperature is kept between 40~90 °C. Its temperature is firstly set at 40 °C for 1 h, and then its temperature is respectively maintained at 50, 60, 70, 80, 90 °C for 15 min. Thereafter, 5 ml distilled water is added into the flask. 2 h later, 70 ml ethanol is added into the flask, which is taken out, and is let stand for 1 h. Then, the mixture is filtered and fully washed using ethanol 2~3 times. Finally, the $Mn_3O_4/G/CB$ composite is obtained, after the filter residue is dried in an oven at 80 °C for 20 h. In the same way, two other $Mn_3O_4/G/CB$ composites are prepared by changing the amount of the graphene and carbon black. The $Mn_3O_4/G/CB$ composites are denoted as $Mn_3O_4/G/CB-a/b$, where 'a' and 'b' are the amount of the graphene and carbon black. Without the addition of the graphene and carbon black, the prepared material is pure Mn_3O_4 .

2.3 Characterization of electrode materials

The morphologies of the carbon black, graphene, $Mn_3O_4/G/CB-0.02/0.01$ composite and pure Mn_3O_4 are investigated using a Tecnai G2 F20 S-TWIN transmission electron microscope (TEM, FEI). X-ray powder diffraction data of the carbon black, graphene, $Mn_3O_4/G/CB-0.02/0.01$ composite and pure Mn_3O_4 are collected using a Rigaku Dmax 2400 X-ray diffractometer.

2.4 Electrochemical test

The electrochemical performance of the electrode materials for supercapacitor is investigated by CV, GCD and EIS techniques using a CHI 760E electrochemical workstation (Shanghai, China) at the ambient temperature (~25 °C). The electrolyte solution 2 M Na_2SO_4 solution, whose pH is adjusted to 10 by KOH solution. The working electrode is manufactured based on the method described in literature [18-20]. In brief, 20 μ l composite ink, prepared by mixing 20 mg tested electrode material, 5 mg carbon black, 4 ml ethanol, 30 μ l PTFE emulsion and 30 μ l Nafion solution (5 wt%, DuPont Corp., USA), is placed on a polished glassy carbon working electrode ($\Phi = 5$ mm) using a microsyringe. An Ag|AgCl electrode and a sheet of platinum (2 cm^2) are respectively employed as the reference electrode and counter electrode.

3. RESULTS AND DISCUSSION

3.1 Electrode materials characterization

Figure 1 indicates the images of the carbon black, graphene, pure Mn_3O_4 and $Mn_3O_4/G/CB-0.02/0.01$ composite. Figure 1a is the TEM image of the carbon black with spherical structure, whose

particles are bonded together. Their average size is about 100 nm. The 2-dimensional (2D) structure of the graphene (the reduced graphene prepared by hydroiodic acid) is displayed in Figure 1b, which shows that the surface area of the graphene is very large, implying that the graphene can provide adequate platform for the growth of the Mn_3O_4 . As can be seen from Figure 1b, there is a large amount of folding on the surface of the RGO, because the overlap between graphene layers or the transformation from the two-dimensional (2D) to 3D of graphene with few layers can decrease the surface energy [21, 22].

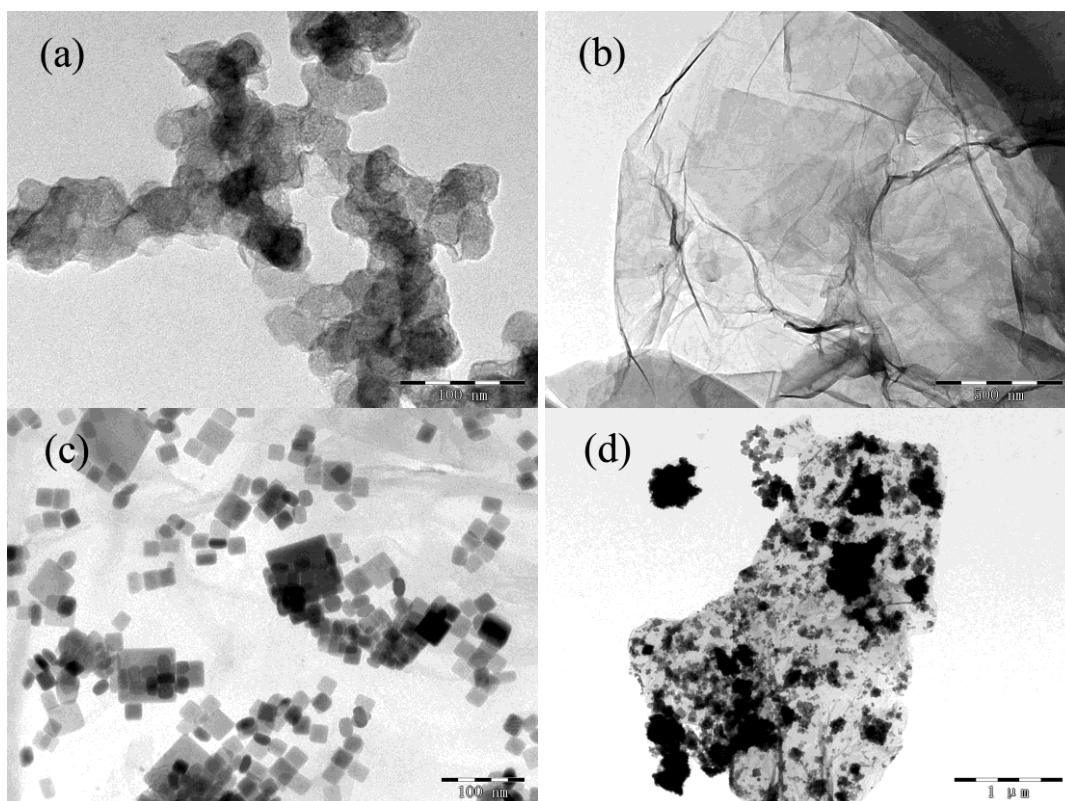


Figure 1. TEM images of the carbon black (a), graphene (b), pure Mn_3O_4 (c), and Mn_3O_4 /G/CB-0.02/0.01 composite (d).

Figure 1c exhibits the images of the nanoparticles, which indicates that the average size is about 10 nm. The TEM image of the Mn_3O_4 /G/CB-0.02/0.01 composite is displayed in Figure 1d, which indicates that, the Mn_3O_4 nanoparticles are arrayed on the surface of the 2D graphene and carbon black.

Figure 2 is the XRD patterns of the carbon black, graphene, pure Mn_3O_4 , and Mn_3O_4 /G/CB-0.02/0.01 composite. As can be seen from Figure 2, the diffraction peaks of the carbon black with high electrical conductivity are located at $2\theta = 26.2$ and 44.3° , which are consistent with the carbon with hexagonal crystal system (JCPDS No. 75-1621). There is a wide diffraction peak between $24\sim 26^\circ$ in the XRD pattern of the graphene.

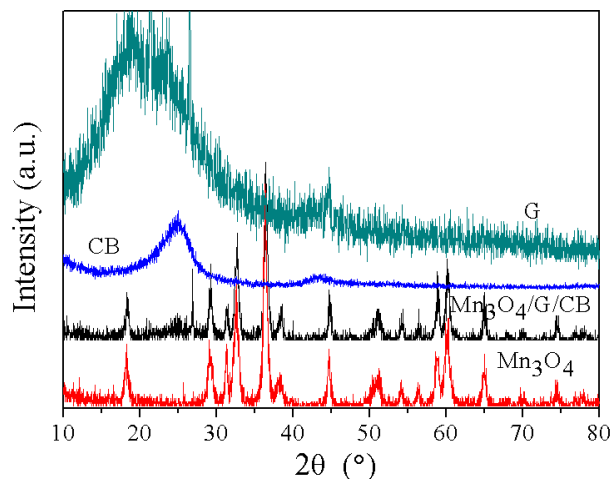


Figure 2. XRD patterns of the carbon black, graphene, pure Mn_3O_4 , and $\text{Mn}_3\text{O}_4/\text{G}/\text{CB}$ -0.02/0.01 composite.

The corresponding layer spacing calculated by Scherrer formula is about 0.34~0.37 nm, which is close to the theoretical standard the natural graphite (0.33 nm) [23]. The [002] diffraction peaks of graphite emerges appears at $2\theta = 26^\circ$; while the [001] diffraction peaks of the graphite oxide is not arise, showing that the amount of the oxygen groups has been greatly reduced in the reduced graphene. The characteristic diffraction peaks of the Mn_3O_4 are located at $2\theta = 18.2, 36.5, 44.4$ and 60.8° in the XRD patterns of the pure Mn_3O_4 and $\text{Mn}_3\text{O}_4/\text{G}/\text{CB}$ -0.02/0.01 composite, which is corresponding to the cubic Mn_3O_4 structure (JCPDS No. 24-0734) [24]. Moreover, the diffraction peak at $2\theta = 26.3^\circ$ in the XRD pattern of the $\text{Mn}_3\text{O}_4/\text{G}/\text{CB}$ -0.02/0.01 composite corresponds to the carbon black. These results suggest that the Mn_3O_4 nanoparticles successfully combined together with the carbon black and graphene.

3.2 Electrochemical study

Figure 3a is the cyclic voltammograms (CVs) of the $\text{Mn}_3\text{O}_4/\text{G}/\text{C}$ -0.02/0.01 composite at different scan rates, which indicates that the CVs at low scan rates maintain a good rectangular shape, showing the reversibility of the kinetics in the charge-discharge process is good. Furthermore, the current response rate in the reverse scan is very quick, implying that the $\text{Mn}_3\text{O}_4/\text{G}/\text{C}$ -0.02/0.01 composite the advantages of low internal resistance and good charge transfer properties. This result is attributed the addition of the carbon black and graphene, which improve the electric conductivity of Mn_3O_4 . With the increase in the scan rate, the CV curve deviates from the rectangle, suggesting the capacitance property of the $\text{Mn}_3\text{O}_4/\text{G}/\text{C}$ -0.02/0.01 composite has weakened. The CVs of the pure Mn_3O_4 composite at different scan rates are shown in Figure 3b, which indicates that a pair of redox peaks can be observed clearly in each CV curve, implying that the pseudocapacitive reaction has happen at this electrode potential range [25,26]. Figure 3c displays The CV curves of the carbon black, graphene, Mn_3O_4 and $\text{Mn}_3\text{O}_4/\text{G}/\text{C}$ -0.02/0.01 composite at the scan rate 200 mV/s.

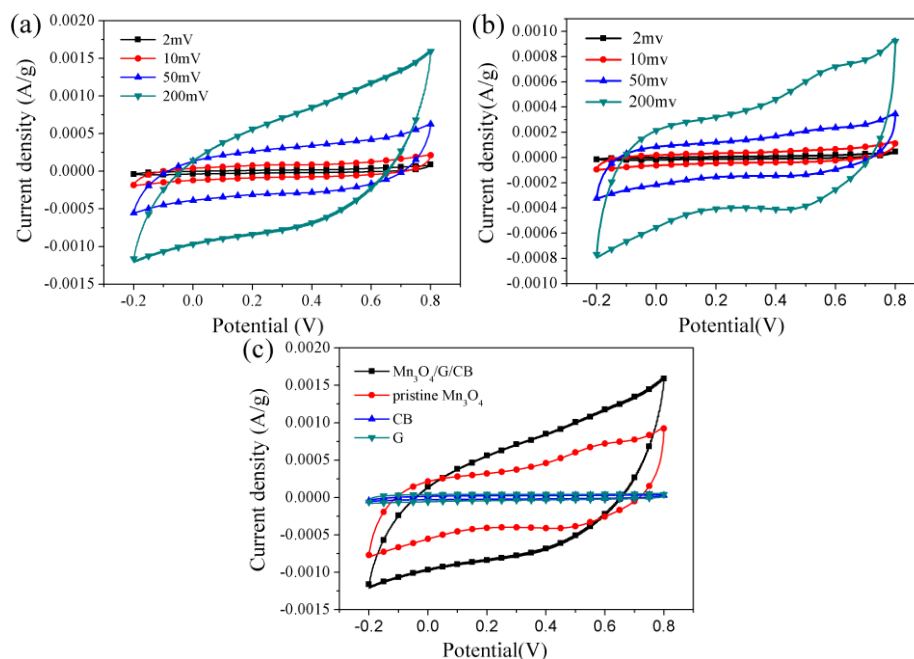


Figure 3. (a) CV curves of the Mn₃O₄/G/C-0.02/0.01 composite at different scan rates. (b) CV curves of the pure Mn₃O₄ composite at different scan rates. (c) CV curves of the carbon black, graphene, Mn₃O₄ and Mn₃O₄/G/C-0.02/0.01 composite at the scan rate 200mV/s.

As can be seen from Figure 3c, the areas of the closed regions formed by the CVs of the carbon black, graphene are negligible, showing these two kinds of conductive carbon materials only have little capacitance. Moreover, the area of the closed region formed by the CV of the Mn₃O₄/G/C-0.02/0.01 composite is great larger compared to Mn₃O₄. These results suggest that the good electric conductive of the graphene and the high surface area of the carbon black are made full use of to enhance the specific capacitance of the Mn₃O₄. Figure 4a and b respectively are the GCD curves of the pure Mn₃O₄ and Mn₃O₄/G/C-0.02/0.01 composite at different current densities. Figure 4a and b shows that the specific capacitance of electrode decreases with the current density, because the slow rate of ions at the low current densities makes the electrode reaction take place on the electrode surface as well as in the bulk phase [27,28]. According to Figure 4a and b, the specific capacitances of the Mn₃O₄/G/C-0.02/0.01 composite and pure Mn₃O₄ calculated by GCD curves at the current densities of 0.1 A/g are 661 and 165 F/g, respectively. The reason that the specific capacitance of the Mn₃O₄/G/C-0.02/0.01 composite is much higher than that of the Mn₃O₄ can be attributed to the addition of the graphene and carbon black. This conclusion is consistent with the cyclic voltammetry test results. The specific capacitances of the Mn₃O₄/G/C-0.02/0.01 composite and pure Mn₃O₄ at different current densities are calculated based on Figure 4a and b. The corresponding data are listed in Table 1. As can be seen from these data, the specific capacitance of the Mn₃O₄/G/C-0.02/0.01 composite is higher than that of the Mn₃O₄ at each current density, even at the big current density of 10 A/g. This result can be observed intuitively from the GCD curves of the carbon black, graphene, pure Mn₃O₄, and Mn₃O₄/G/CB-0.02/0.01 composite at the current density of 3 A/g, which is indicated in Figure 4c. The effect of the mass ratio between the graphene and carbon black on the specific capacitance of the Mn₃O₄/G/CB composite is investigated at the current densities of 3 and 0.3 A/g.

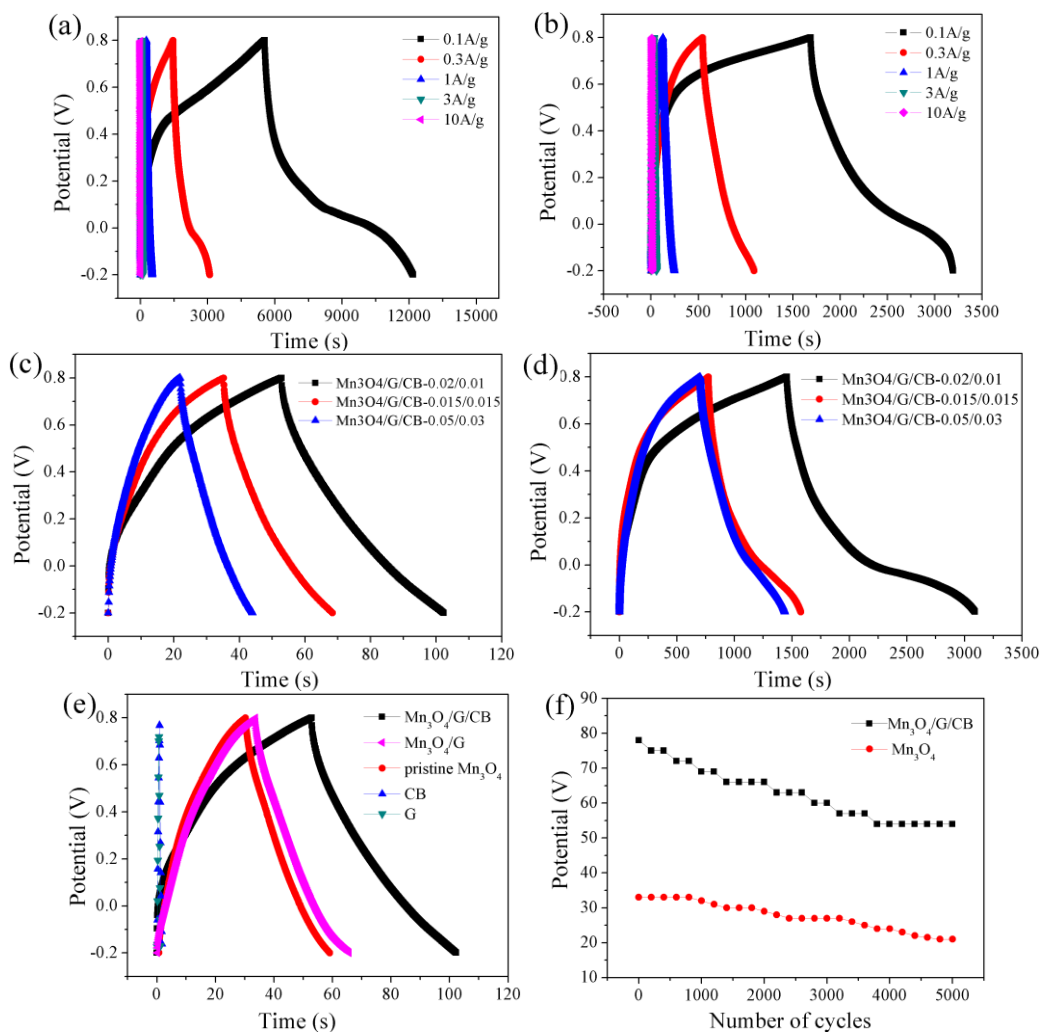


Figure 4. (a) GCD curves of the $Mn_3O_4/G/C-0.02/0.01$ composite at different current densities. (b) GCD curves of the pure Mn_3O_4 at different current densities. (c) GCD curves of the $Mn_3O_4/G/C-0.02/0.01$, $Mn_3O_4/G/C-0.015/0.015$ and $Mn_3O_4/G/C-0.05/0.03$ composites at the current density of 3 A/g. (d) GCD curves of the $Mn_3O_4/G/C-0.02/0.01$, $Mn_3O_4/G/C-0.015/0.015$ and $Mn_3O_4/G/C-0.05/0.03$ composites at the current density of 0.3 A/g. (e) GCD curves of the carbon black, graphene, pure Mn_3O_4 , and $Mn_3O_4/G/CB-0.02/0.01$ composite at the current density of 3 A/g. (f) Cycle curves of the pure Mn_3O_4 and $Mn_3O_4/G/CB-0.02/0.01$ composite at the current density of 30 A/g for 5000 circles.

The corresponding GCD curves are displayed in Figure 4 d and e, which suggest that the best mass ratio between the graphene and carbon black is 2:1. The possible reason is that this ratio can effectively avoid the irreversible aggregation of graphene sheets, as well as make the most of the strengths of the graphene and carbon black to improve the specific capacitance of the Mn_3O_4 . Figure 4f exhibits the cycle curves of the pure Mn_3O_4 and $Mn_3O_4/G/CB-0.02/0.01$ composite at the current density of 30 A/g for 5000 circles. It is found from Figure 4f that, the specific capacitance retention rate of the $Mn_3O_4/G/CB-0.02/0.01$ composite is 69.2%, and its capacitance remains stable at 54 F/g; while the specific capacitance retention rate and the final capacitance of the pure Mn_3O_4 are 63.6% and 21 F/g, respectively. Moreover, the specific capacitance of $Mn_3O_4/G/CB-0.02/0.01$ composite is higher

than that of the reported Mn₃O₄ composites [29,30], due to the close integration of the CB, graphene and Mn₃O₄. These results imply that the addition of the graphene and carbon black not only increases the capacitance of the composite, but also greatly improves its cycling stability.

Table 1 The specific capacitance of the Mn₃O₄ and Mn₃O₄/G/CB-0.02/0.01 at different current densities.

Current density (A/g)	0.1	0.3	1	3	10
Capacitance (F/g)					
Mn ₃ O ₄ /G/CB	661	474	270	150	70
Mn ₃ O ₄	165	150	120	84	55

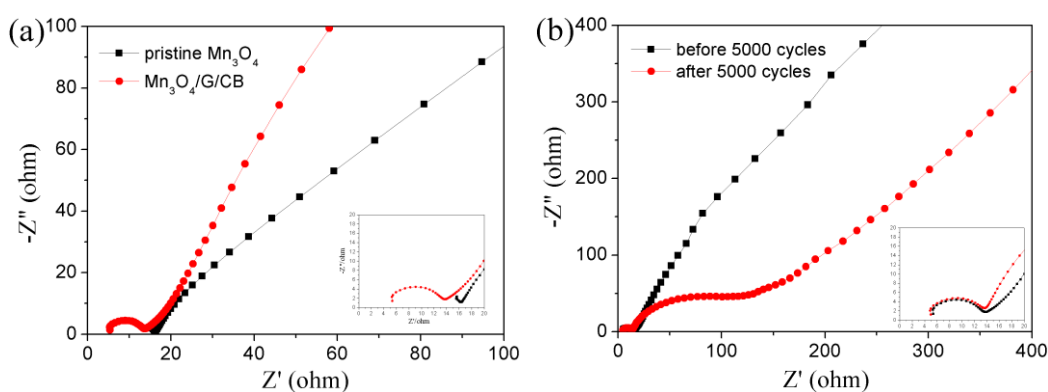


Figure 5. (a) EIS curves of the pure Mn₃O₄, and Mn₃O₄/G/CB-0.02/0.01 composite. (b) EIS curves of the Mn₃O₄/G/CB-0.02/0.01 composite before and after 5000 charge-discharge cycles at 30 A/g.

The EIS curves of the pure Mn₃O₄, and Mn₃O₄/G/CB-0.02/0.01 composite are displayed in Figure 5a, in which the EIS curves in the high frequency zone are shown as an insert. As is shown in Figure 5a, the estimated electrolyte resistances of the pure Mn₃O₄, and Mn₃O₄/G/CB-0.02/0.01 composite respectively are 9.9 and 6 Ω, and the estimated charge transfer resistance of the pure Mn₃O₄, and Mn₃O₄/G/CB-0.02/0.01 composite are respectively 9.9 and 6 Ω. These results indicate that the addition of the graphene and carbon black significantly decreases the electrolyte resistance and charge transfer resistance of the pure Mn₃O₄. The EIS curves of the Mn₃O₄/G/CB-0.02/0.01 composite before and after 5000 charge-discharge cycles at 30 A/g are shown in Figure 5b, where the EIS curves in the high frequency zone are exhibited as an illustration. It is found from Figure 5b that, the electrolyte resistance and charge transfer resistance of the Mn₃O₄/G/CB-0.02/0.01 composite has barely budged. However, the slope of the EIS curve in the low frequency region decreases obviously, suggesting that the Warburg resistance of the CNTs/RGO/MnO₂ composite increases after 5000 charge-discharge cycles under the large current density of 30 A/g [31,32].

4. CONCLUSION

The reduced graphene synthesized by the graphene oxide prepared by a modified Hummers method using hydroiodic acid as the reducing reagent. The $\text{Mn}_3\text{O}_4/\text{G}/\text{CB}$ composites are synthesized by the prepared graphene, carbon black and manganous acetate using a facile chemical method. The results of TEM test display that, the cubic Mn_3O_4 nanoparticles are successfully arrayed on the surface of the 2D graphene and carbon black. The electrochemical test results indicate that the specific capacitance of the $\text{Mn}_3\text{O}_4/\text{G}/\text{C}-0.02/0.01$ composite is much higher than that of the Mn_3O_4 , due to the improvement in the electric conductivity of the composite caused by the carbon black and graphene. Moreover, the specific capacitance of the $\text{Mn}_3\text{O}_4/\text{G}/\text{CB}-0.02/0.01$ composite is highest among the $\text{Mn}_3\text{O}_4/\text{G}/\text{CB}$ composites, because this ratio effectively avoids the irreversible aggregation of graphene sheets, as well as makes the most of the strengths of the graphene and carbon black to improve the specific capacitance of the Mn_3O_4 . Furthermore, the specific capacitance retention rate of the $\text{Mn}_3\text{O}_4/\text{G}/\text{CB}-0.02/0.01$ composite after 5000 circles at the big current density of 30 A/g is far higher compared to Mn_3O_4 , implying that the addition of the graphene and carbon black not only increases the capacitance of the composite, but also greatly improves its cycling stability. After 5000 charge-discharge cycles at 30 A/g, the electrolyte resistance and charge transfer resistance of the $\text{Mn}_3\text{O}_4/\text{G}/\text{CB}-0.02/0.01$ composite has barely budged. Therefore, the $\text{Mn}_3\text{O}_4/\text{G}/\text{CB}$ composite has the potential to be employed as a supercapacitor electrode material.

ACKNOWLEDGEMENTS

This work is supported by the Natural Science Foundation of Shanxi (2014011017-2) and Scientific and Technological Innovation Programs of Higher Education Institutions in Shanxi (STIP, 2014113).

References

1. N. B. Trung, T. V. Tam, D. K. Dang, K. F. Babu, E. J. Kim, J. Kim and W. M. Choi, *Chem. Eng. J.*, 264 (2015) 603.
2. F. Ran, H. Fan, L. Wang, L. Zhao, Y. Tan, X. Zhang, L. Kong and L. Kang, *J. Energy Chem.*, 22 (2013) 928.
3. M. M. Thackeray, *Prog. Solid State Ch.*, 25 (1997) 1.
4. X. H. Lv, W. Lv, W. Wei, X. Y. Zheng, C. Zhang, L. J. Zhi and Q. H. Yang, *Chem. Commun.*, 51 (2015) 3911.
5. B. G. S. Raj, R. N. R. Ramprasad, A. M. Asiri, J. J. Wu and S. Anandan, *Electrochim. Acta*, 156 (2015) 127.
6. C. M. Park and K. J. Jeon, *Chem. Commun.*, 47 (2011) 2122.
7. W. M. Zhang, J. Chen, A. I. Minett, G. F. Swiegers, C. O. Too and G. G. Wallace, *Chem. Commun.*, 46 (2010) 4824.
8. S. Oke, M. Yamamoto, K. Shinohara, H. Takikawa, H. Xiaojun, S. Itoh, T. Yamaura, K. Miura, K. Yoshikawa, T. Okawa and N. Aoyagi, *Chem. Eng. J.*, 146 (2009) 434.
9. Z. Y. Huang, G. C. Liang, L. and Z. Fan, *Chem. J. Chinese U.*, 32 (2011) 2630.
10. G. K. Yang and K. Q. Ding, *Chem. J. Chinese U.*, 31 (2010) 994.
11. Q. Li, X. F. Lu, H. Xu, Y. X. Tong and G. R. Li, *Acs Appl. Mater. Inter.*, 6 (2014) 2726.
12. S. H. Yang, X. F. Song, P. Zhang and L. Gao, *Acs Appl. Mater. Inter.*, 5 (2013) 3317.

13. J. Y. Qu, Y. J. Li, C. P. Li, L. Shi, G. H. Shao and F. Gao, *New Carbon Mater.*, 29 (2014) 186.
14. G. Yu, L. Hu, M. Vosgueritchian, H. Wang, X. Xie, J. R. McDonough, X. Cui, Y. Cui and Z. Bao, *Nano Lett.*, 11 (2011) 2905.
15. Z. Yu, B. Duong, D. Abbitt and J. Thomas, *Adv. Mater.*, 25 (2013) 3302.
16. J. Y. Luo and Y. Y. Xia, *Adv. Funct. Mater.*, 17 (2007) 3877.
17. W. S. Hummers and R. E. Offeman, *J. Am. Chem. Soc.*, 80 (1958) 1339.
18. S. Yan, L. Gao, S. Zhang, W. Zhang, Y. Li and L. Gao, *Electrochim. Acta*, 94 (2013) 159.
19. S. Yan, L. Gao, S. Zhang, L. Gao, W. Zhang and Y. Li, *Int. J. Hydrogen Energy*, 38 (2013) 12838.
20. S. Yan, S. Zhang, W. Zhang, J. Li, L. Gao, Y. Yang and Y. Gao, *J. Phys. Chem. C*, 118 (2014) 29845.
21. X. Du, C. Zhou, H. Y. Liu and Y. W. Mai, *J. Power Sources*, 241 (2013) 460.
22. X. L. Li, G. Y. Zhang, X. D. Bai, X. M. Sun, X. R. Wang, E. Wang, and H. J. Dai, *Nat. Nanotechnol.*, 3 (2008) 538.
23. M. Yu, J. Chen, Y. Ma, J. Zhang, J. Liu, S. Li and J. An, *Appl. Surf. Sci.*, 314 (2014) 1000.
24. J. Duan, S. Chen, S. Dai and S. Z. Qiao, *Adv. Funct. Mater.*, 24 (2014) 2072.
25. M. S. Wu, Z. S. Guo and J. J. Jow, *J. Phys. Chem. C*, 114 (2010) 21861.
26. Y. Y. Gao, S. L. Chen, D. X. Cao, G. L. Wang and J. L. Yin, *J. Power Sources*, 195 (2010) 1757.
27. J. H. Kim, K. Zhu, Y. F. Yan, C. L. Perkins and A. Frank, *Nano Lett.*, 10 (2010) 4099.
28. C. J. Yu, C. Masarapu, J. P. Rong, B. Q. Wei and H. Q. Jiang, *Adv. Mater.*, 21 (2009) 4793.
29. G. R. Xu, J. J. Shi, W. H. Dong, Y. Wen, X. P. Min and A. P. Tang, *J. Alloy. Compd.*, 630 (2015) 266.
30. R. T. Dong, Q. L. Ye, L. L. Kuang, X. Lu, Y. Zhang, X. Zhang, G. J. Tan, Y. X. Wen and F. Wang, *ACS Appl. Mater. Inter.*, 5 (2013) 9508.
31. T. C. Girija and M. V. Sangaranarayanan, *J. Power Sources*, 156 (2006) 705.
32. W. C. Chen and T. C. Wen, *J. Power Sources*, 117 (2003) 273.